

# Modeling Biological Membrane and Red Blood Cells by Coarse-Grained Particle Method

He Li<sup>1\*</sup>, Hung-yu Chang<sup>1</sup>, Jun Yang<sup>2</sup>, Lu Lu<sup>1</sup>, George Lykotrafitis<sup>3</sup>

<sup>1</sup>Division of Applied Mathematics, Brown University, Providence,  
Rhode Island, 02912, U.S.A

<sup>2</sup>Department of Materials Science and Engineering, Massachusetts Institute of  
Technology, Cambridge, Massachusetts, 02139, U.S.A.

<sup>3</sup>Department of Mechanical Engineering, University of Connecticut, Storrs,  
Connecticut, 06269, USA

## ABSTRACT

In this work, we review previously developed coarse-grained (CG) particle models for biological membrane and red blood cells (RBCs) and discuss the advantages of the CG particle method over the continuum and atomic simulations on modeling biological phenomena. CG particle models can largely increase the length scale and time scale of atomic simulations by eliminating fast degrees of freedom while preserving the mesoscopic structures and properties of the simulated system. On the other hand, CG particle models can be used to capture microstructural alternations in diseased RBCs and simulate topological changes of biological membrane and RBCs, which are major challenges to typical continuum representations of membrane and RBCs. The power and versatility of the CG particle methods are demonstrated through simulating the dynamical processes involving significant topological changes, such as lipid self-assembly, vesicle fusion and membrane budding.

---

\*Corresponding author He Li, Ph.D E-mail: [he\\_li@brown.edu](mailto:he_li@brown.edu)

## 1. Introduction

Biological membrane is a vital component of living cells as it helps maintain the structural integrity of the cells and their organelles <sup>[1, 2]</sup>. The plasma membrane separates the cytoplasm from the extracellular environment and the internal membranes separate the cytoplasm from the lumen of the organelles. Biomembrane is also important for various cell functions <sup>[3]</sup>. Transport vesicles that carry materials from the extracellular medium or from the lumen of an organelle, are formed by budding off from a membrane. These vesicles deliver their load via fusion with the membrane of the target organelle <sup>[4]</sup>. Cell membrane also plays a key role in such processes as cell differentiation, cell–cell adhesion, and cell migration <sup>[1]</sup>. Biological membrane is constituted mostly by a wide variety of lipids and protein molecules. A lipid molecule consists of a hydrophilic polar head and two hydrophobic hydrocarbon chains. When introduced into an aqueous environment, lipid molecules spontaneously aggregate into bilayer and then form vesicles due to the hydrophobic effect. Biomembrane has a two-dimensional (2D) fluid-like structure embedded in three-dimensional (3D) space. Although the membrane is only a few nanometers ( $\sim 5$  nm) thick, the size of vesicles can be up to micrometers. Open, sheet-like configurations are less frequently seen because the hydrophobic edges would incur a large free energy penalty <sup>[2]</sup>.

Red blood cells (RBCs) are unique amongst eukaryotic cells as they bear no nucleus or cytoplasmic structures or organelles <sup>[5]</sup>. Therefore, the structural properties are linked to the cell membrane. In addition to the lipid bilayer and integral proteins, RBC membrane possesses a 2D cytoskeleton tethered to the lipid bilayer. The RBC membrane cytoskeleton consists of spectrin tetramers, which are connected at the actin junctional complexes, forming a 2D sixfold structure. The cytoskeleton is connected to the lipid bilayer via ‘‘immobile’’ band-3 proteins at the spectrin-ankyrin binding sites and via glycophorin protein at the actin junctional complexes <sup>[5]</sup>. Lipid bilayer resists bending but cannot sustain static in-plane shear stress because the lipids and most of the integral proteins can diffuse freely within the membrane to relax the shear stress. The stiffness and rheological deformation resistance of the RBCs arise primarily from the cytoskeleton. Given this particular membrane structure, RBCs have remarkable deformability which allows them to undergo repeated severe deformation when traveling through small blood vessels and organs <sup>[6]</sup>.

In spite of the significant advances made in computing power in the past few decades, it is still computationally prohibitive or impractical to perform atomistic simulations on cell membrane at time scales and length scales that can be used to directly compare with typical laboratory experimental studies. The atomistic simulation techniques are limited by the number of atoms/molecules involved, typically  $10^4 \sim 10^8$  corresponding to a length scale on the order of tens of nanometers. On the other hand, the maximum time step in atomistic simulations is limited by the smallest oscillation period of the fastest atomic motions in a molecule, which is typically several femtoseconds ( $10^{-15}$  s). Owing to the prohibitive computational cost, most atomistic membrane models have been limited to the study of only a few hundred lipids or single proteins for a period of a few nanoseconds <sup>[7-12]</sup>.

At the opposite end of the length scale and time scale spectrums, continuum models based on membrane elasticity <sup>[13-15]</sup> have been adopted to elucidate vesicle shape transitions and to estimate thermal fluctuations of fluid membranes at length scales much larger than the bilayer thickness <sup>[16, 17]</sup>. Boundary integral method <sup>[18-21]</sup> and immersed boundary method <sup>[22-25]</sup> are two popular ways to simulate RBCs based on the assumptions that RBC membrane and embedding fluids are homogeneous materials. These continuum-based RBC models facilitate the study of single cell dynamics, such as tank-threading <sup>[26]</sup>, RBC passing splenic slit <sup>[27]</sup>, or blood flow on macroscopic length and time scales <sup>[28, 29]</sup>. Although the continuum-based RBC models provide an accurate description of RBC deformation at cellular level, they are not able to describe mesoscopic- and microscopic-scale phenomena, such as representing the structural defects in the RBC cytoskeleton, or capture the topological changes of membrane or RBCs, such as self-assembling, fusion of lipid vesicles and membrane budding.

The limitations of atomistic simulations and continuum approaches, along with the practical needs to treat the heterogeneous nature of RBC membranes have motivated a continual search for coarse-grained (CG) particle models that bridge atomistic and continuum models <sup>[11, 30-52]</sup>. CG particle models can substantially simplify the atomistic dynamics by eliminating fast degrees of freedom while preserving the mesoscopic structures and properties of the simulated system <sup>[53]</sup> and it has been applied broadly in polymer dynamics <sup>[54-60]</sup> and biological fibers <sup>[61-67]</sup>. In the following sections, we will review the previously developed biological membrane models, RBC membrane models and RBC whole cell models and demonstrate their power and versatility in simulating the lipid self-assembly, vesicle fusion and membrane budding.

## 2. Coarse-grained particle model

### 2.1 Biological membrane models

CG membrane models typically involve grouping a cluster of atoms in a phospholipid molecule into CG particles as phospholipids are the most abundant membrane lipids which have a polar head group and two hydrophobic hydrocarbon tails. An atomic model for a phospholipids molecule is shown in Fig. 1(a). As a result, each lipid molecule is treated as a short chain of CG particles. Distinctions among the various CG membrane models arise from levels of coarse-graining, which are determined by the targeted problems of the simulation. Markvoort et al. <sup>[46]</sup> introduced a coarse-grained molecular dynamics (CGMD) model for lipid molecules where two chains of four CG particles represent the two hydrophobic tails and another chain of four CG particles represents the lipid headgroup, as shown in Fig.1 (b). The authors used two types of lipids to introduce asymmetry in the lipid bilayers. At a higher level of coarse-graining, Wang and Frenkel <sup>[44]</sup> proposed a membrane model where each lipid molecule was represented by only three CG particles with one particle being hydrophilic head and the other two being hydrophobic tails (see Fig.1 (c)). A number of CGMD membrane models were developed following similar strategy <sup>[31, 32, 34-36, 39, 40, 45, 68]</sup>. To achieve a high level of coarse-graining, Yuan et al. <sup>[69]</sup> coarse-grained a group of lipid molecules to one single CG particle and built a one-particle thick lipid bilayer model (see Fig.1 (d)). The hydrophilic and hydrophobic properties of the lipid molecules are represented by a directional vector.

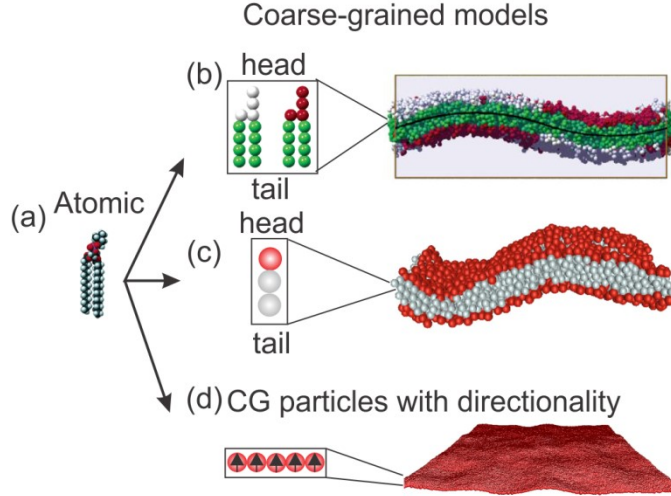


Figure 1. (a) An atomic model for a lipid molecule. (b) A CGMD model representing a lipid molecule by three chains of particles. Two four-particle chains represent the tails of lipid molecule and one four-particle chain represents the head. Adapted from Ref <sup>[46]</sup>. (c) A CGMD model representing a lipid molecule by a chain of three CG particles. Two CG particles represent the tails of lipid molecule and one CG particle represents the head. Adapted from Ref <sup>[44]</sup> (d) One-particle thick lipid bilayer model where each CG particle carries a directional vector and it represents a lump of lipid molecules<sup>[69]</sup>.

CG particle model for biological membrane can also be generally categorized into explicit solvent and implicit solvent (solvent-free) schemes <sup>[30, 45, 49]</sup>. Explicit solvent schemes employ the hydrophobic interactions between lipids and solvent particles (a water molecule or a group of several water molecules) to stabilize the 2D lipid membrane <sup>[35, 43]</sup>. Explicit solvent models frequently employ dissipative particle dynamics (DPD), a very efficient method that represents a large volume of the solvents with a soft bead, thus significantly accelerating the computations <sup>[70-72]</sup>. There are three types of forces present in DPD models: a conserved soft repulsion force, pairwise dissipation forces and pairwise random forces. The balance of dissipation and random forces naturally provides the thermostat for the DPD model. DPD method preserves the momentum of individual particles and thus provides correct hydrodynamic behavior. In addition to increased length scale, DPD simulations use a longer timestep due to the application of soft repulsion forces. The explicit solvent approach can significantly increase the computational time as the solvent particles are required to fill a 3D simulation box and their number increases rapidly with the size of the simulated system. Solvent-free approaches are inherently advantageous because they result in much larger accessible length and time scales <sup>[45, 73]</sup>. In implicit solvent schemes, the solvent particles are not directly represented in the simulation and their effect is taken into account by effective multibody interaction potentials, based on either the local particle density <sup>[31, 34, 44]</sup>, or by applying different pair-potentials between particles representing the hydrophobic tails and particles representing the hydrophilic head of the lipids <sup>[36, 39, 40]</sup>. Difficulties in developing solvent-free CGMD models for lipid membranes lie in the incorporation of hydrophobic interactions via multibody potentials to capture the hydrophobic behavior of

the lipid molecules and the formation of fluid membrane sheets. The classical LJ type potentials introduce large restoring forces near the equilibrium distance between two neighboring particles and generally yield either ordered high-density solid phase at low temperatures or disordered low-density gas phase at high temperatures. A solution to the problem is to utilize a pair potential between tail beads softer than the LJ-type potentials to stabilize the membrane in the fluid phase while employing LJ type potentials for all the other inter-bead interactions <sup>[40]</sup>. Along this line, Drouffe et al. <sup>[31]</sup> and Noguchi et al. <sup>[47]</sup> developed one-particle-thick, CGMD models to simulate biological membranes. In Drouffe's model, the interactions between CG particles are described by a LJ type pair potential, but it not only depends on the distance between the particles but also on their directionality, whereas Noguchi et al. introduced a multibody potential that eliminated the need of the rotational degree of freedom <sup>[47]</sup>. Yuan et al. introduced membrane model with a similar approach, but instead of applying a LJ type potential, a soft-core potential was used to better illustrate the particle self-diffusion <sup>[69]</sup>.

## 2.2 Lipid self-assembling and membrane fusion

Self-assembly processes of lipids from a randomly dispersed state to an ordered bilayer structure have been captured by CG particle models <sup>[37, 46, 74, 75]</sup>. Starting from a random dispersion, lipids rapidly aggregate into micelles and small bilayers also referred to bicelles. Subsequently, these small aggregates merge into a large disklike bilayer. In order to minimize the line tension arising at the bilayer edge, this bilayer tends to seal and form a vesicle by gradually encapsulating water, see a self-assembly process of lipids in Fig. 2. In fact, such bent lamellar structure is essential to cell membrane related processes, especially during exo- and endocytosis. For entropic reasons, a bilayer does not stay at a simply planar state, it exhibits thermal fluctuations (undulations), and its bending rigidity is responsible for manipulating the fluctuations in the average position of the bilayer surface <sup>[76]</sup>. Although a vesicle can persist for a long time, it is merely in a metastable state instead of a thermodynamic equilibrium state. This is attributed to the implicitly higher pressure and chemical potential of water in the interior domain than those in the exterior domain of a vesicle <sup>[75]</sup>. In addition, the smaller the vesicle is the larger the pressure difference exists, and thus, small vesicles are thermodynamically less stable against fusion than the larger ones.

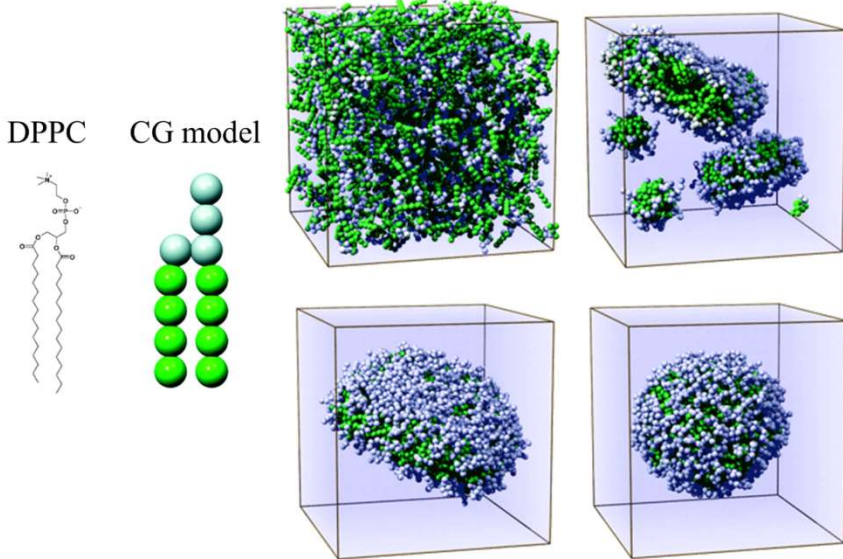


Figure 2. A randomly dispersed DPPC (dipalmitoylphosphatidylcholine) lipids spontaneously form an enclosed bilayer structure (a vesicle), and the snapshots of the evolutionary process are from the work by Markvoort et al. [43].

Lipids in bilayer membrane can be either a solid-ordered state or a liquid-disordered state. It is known that lipid bilayers exhibit a phase transition from a gel phase to a liquid phase as the temperature increases [77, 78]. For some lipids, e.g. DPPC and DMPC (dimyristoylphosphatidylcholine), there could exist an intermediate state (ripple phase) between the gel and liquid phases [79], see Fig 3, and the ripple phase can be either symmetric or asymmetric, depending on the cooling rate from the liquid state down to a crystalline structure [80]. Different phase behavior of a lipid bilayer affects its membrane structure and mechanical properties, and therefore the functioning of biological membranes is also temperature-dependent. In addition to the change of molecular volume (or area per lipid) and heat capacity with temperature as shown in Fig 3, several DPD simulations [81-83] have demonstrated that the membrane thickness of the lipid bilayer ( $h$ ) and the orientation of lipid tail ( $S$ ) can be a function of the temperature ( $T$ ) and the main transition temperature ( $T_m$ ) is located right at the inflection point of  $h(T)$  and  $S(T)$ . CGMD membrane models can facilitate the estimation of membrane physical properties as well. For example, the water permeability of the modeled membrane was predicted by the release rate of the luminal substance. Wu et al. [82, 84] have showed that the water permeability of the bilayer membrane grows exponentially with increasing  $T$  for  $T > T_m$  and their simulation results agreed well with the experimental measurements [84]. In addition, the bending modulus can be obtained from the undulation spectrum of bilayer membrane. The intensity  $I = \langle u^2 \rangle$  of the undulations with amplitude  $u$  obey  $q^4$  behavior in the long wavelength regime, i.e.  $I \propto k_B T (A k_c q^4)^{-1}$ , where  $A$  is the membrane area,  $q$  is wavenumber, and  $k_c$  denotes the bending modulus. By fitting the equation to the simulation data, Marrink et al. [85] obtained  $k_c = 4 \pm 2 \times 10^{-20} \text{ J}$  close to the value  $5.6 \pm 0.6 \times 10^{-20} \text{ J}$  obtained experimentally for DMPC lipids [86].

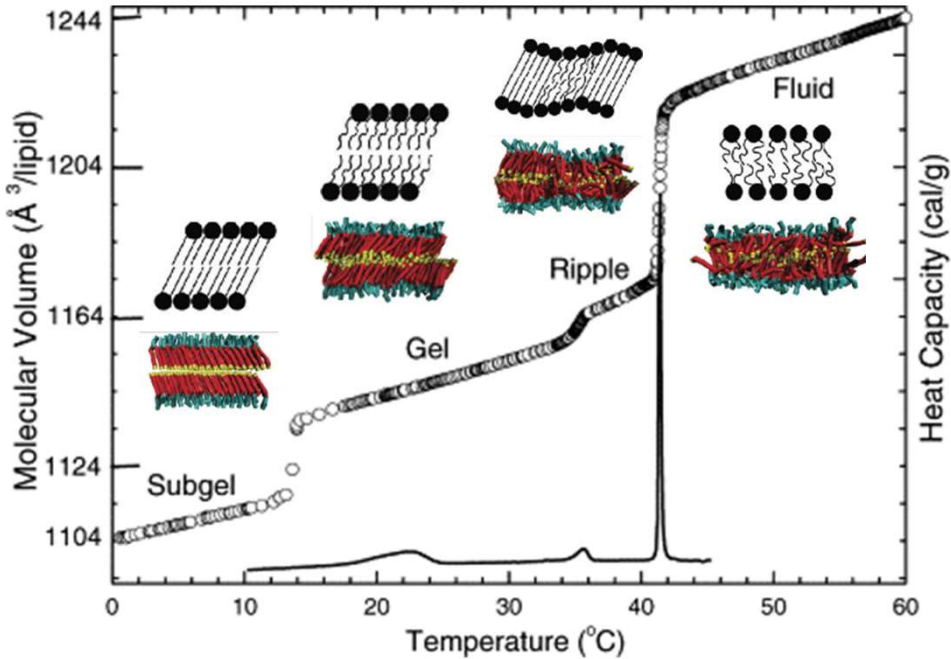


Figure 3. Phase transition of DPPC bilayers in excess water with experimental data of molecular volume (open circles) and heat capacity (solid line) showing a sharp transition from ripple to fluid (liquid) phases at  $T_m \sim 41$  °C. Data is adopted from Refs. [79, 87, 88]. Representative diagrams of various lipid phases are from the DPD work of Rodgers et al. [81], and the modeled lipids are colored in cyan for lipid heads, red for lipid tails, and yellow for the final bead in each tail in order to better display the relative tail order in each phase.

Vesicle fusion is a principal function of cells to communicate and execute a series of bio-physical activities from vesicular trafficking to cell-cell fusion [89]. In addition, lipids fusion is utilized to several technological applications such as drug delivery [90] and the surface modifications of supported lipid bilayer for biosensors [91, 92]. Many in vitro fusion experiments have been performed with lipid vesicles and the dynamic process is in milliseconds and micrometer length scale [93, 94]. However, the molecular structures and transitions during fusion cannot be captured and visualized by currently experimental techniques. On the other hand, numerical framework can allow itself to elucidate the vesicle fusion in more detail. Many pathways have been reported for the fusion processes of lipid vesicles with the help of CG modeling, and the stalk–pore hypothesis (original stalk model) is widely used [38, 95-99], see also Fig. 4 (left). First emergence a neck-like structure (usually regarded as a stalk) initiated by splayed and tilted lipids connects the outer monolayers of two approaching vesicles. Then the stalk grows rapidly to form a hemifusion diaphragm (HD), which has thickness equal to a bilayer thickness in the case of lipid bilayer fusion. The luminal contents enclosed by each vesicles still remain separated in the HD stage. Finally, the pores are generated to end up the fusion process. By using CG lipid model, Marrink et al. [38] found that the speed of stalk formation and the opening of the fusion pore can be modulated by altering the lipid composition.

Another pathway for lipid fusion is called the direct stalk–pore model (modified stalk model)<sup>[98-102]</sup>, as shown in Fig. 4 (right). Similar to the original stalk model, the modified one is defined when there is no evident HD stage during the fusion. It occurs usually when vesicles are under high membrane tension and the pores are originated from the radially expanding stalk. Both the original and modified stalk models are applicable to the fusion of vesicles formed by phospholipids and lipid-like copolymers.

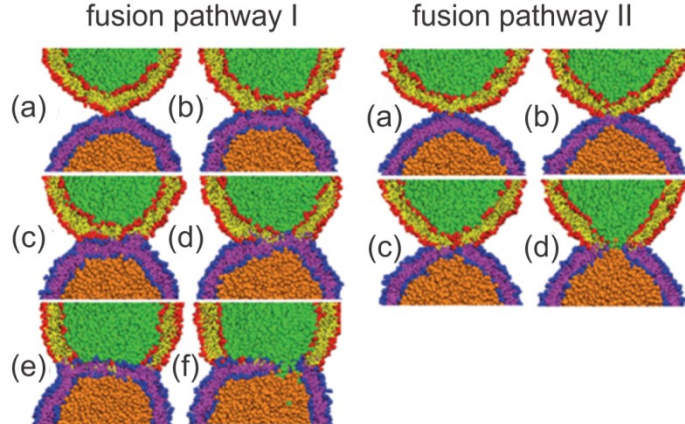


Figure 4. Fusion pathway I (left) for the low tension regime follows original stalk model with the fusion sequence: (a) kissing contact, (b) adhesion, (c) single-bilayer pore formation near the edge of the contact zone, (d) single-bilayer rupture, (e) hemifusion, and (f) fusion pore opening. Fusion pathway II (right) for the high tension regime belongs to a modified stalk model with the fusion sequence: (a) kissing contact, (b) stalk formation, (c) transmembrane fusion pore formation, and (d) fusion pore opening. Upper vesicle has red lipid heads, yellow tails, and green luminal contents, while the lower one has blue lipid heads, purple tails, and gold luminal contents. Simulation snapshots are from Ref. <sup>[98]</sup>.

### 2.3 RBC membrane models

The aforementioned CG particle membrane models only simulate the lipid bilayer without considering the membrane cytoskeleton and thus limit their applications in the study of the biological problems regarding the RBC membrane, such as interactions between the cytoskeleton and the lipid bilayer, and between the cytoskeleton and diffusing membrane proteins. To model membrane for RBCs, Li et al. introduced the a two-component RBC membrane model by combining a cytoskeleton model with lipid bilayer model<sup>[103]</sup>. The cytoskeleton model is comprised of particles that represent actin junctional complexes, which are connected by the WLC potentials to represent spectrin filaments. Although this two-component model exhibits membrane shear modulus that is comparable with experimental measurements, the implicit representation of the spectrin filaments by WLC potential did not allow it to consider the interactions between the spectrin filaments and the lipid bilayer. Therefore, Li et al.<sup>[104]</sup> extended this two-component RBC membrane model by representing spectrin filaments explicitly by CG particles<sup>[105]</sup>. This modified membrane model describes the RBC membrane as a two-component system, including the cytoskeleton and the lipid bilayer. The lipid bilayer is represented by three types of CG particles and the cytoskeleton is represented by two

types of CG particles (see Fig. 5). The cytoskeleton consists of the hexagonal spectrin network and actin junctions. The actin junctions represented by the black particles (see Fig.5), are connected to the lipid bilayer via glycophorin (yellow particles). The spectrin filament is represented by 39 spectrin particles (grey particles) connected by unbreakable springs. The spring potential,  $u_{\text{cy}}^{\text{s-s}}(r) = k_0(r - r_{\text{eq}}^{\text{s-s}})^2 / 2$ , with equilibrium distance  $r_{\text{eq}}^{\text{s-s}} = L_{\text{max}} / 39$ , where  $L_{\text{max}}$  is the contour length of the spectrin ( $\sim 200$  nm) and  $r_{\text{eq}}^{\text{s-s}} \geq 5$  nm.

The spectrin chain is connected to the band-3 particles (white particles). The two ends of the spectrin chains are connected to the actin junction via spring potential,  $u_{\text{cy}}^{\text{a-s}}(r) = k_0(r - r_{\text{eq}}^{\text{a-s}})^2 / 2$  where the equilibrium distance  $r_{\text{eq}}^{\text{a-s}} = 10$  nm. The spring constant  $k_0 = 57 \varepsilon/\sigma^2$ . The spectrin particles, which are not connected by the spring potential, interact with each other via the repulsive part of the L-J potential

$$u_{\text{rep}}(r_{\text{ij}}) = \begin{cases} 4\varepsilon \left[ \left( \frac{\sigma}{r_{\text{ij}}} \right)^{12} - \left( \frac{\sigma}{r_{\text{ij}}} \right)^6 \right] + \varepsilon & r_{\text{ij}} < R_{\text{cut,LJ}} \\ 0 & r_{\text{ij}} > R_{\text{cut,LJ}} \end{cases} \quad (1)$$

where  $\varepsilon$  is the energy unit and  $\sigma$  is the length unit.  $r_{\text{ij}}$  is the distance between the spectrin particles. The cutoff distance of the potential  $R_{\text{cut,LJ}}$  is chosen to the equilibrium distances  $r_{\text{eq}}^{\text{s-s}}$  between the spectrin particles.

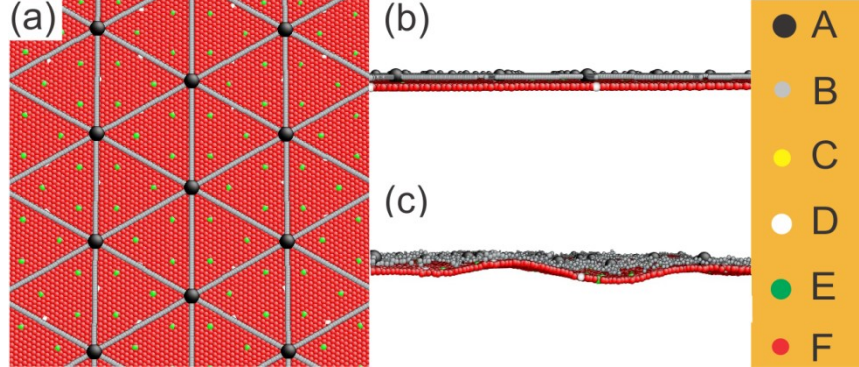


Figure 5. (a) top view and (b-c) side views of two-component RBC membrane model. “A” type particles represent actin junctions. “B” type particles represent spectrin proteins. “C” type particles represent glycophorin proteins. “D” type particles represent band-3 complex that are connected to the spectrin network. “E” type particles represent band-3 complex that are not connected to the network. “F” type particles represent lipid particles.

Three types of CG particles are introduced to represent lipid bilayer and transmembrane proteins (see Fig. 5). The red color particles represent a cluster of lipid molecules, which have a diameter of 5 nm. The yellow particles denote glycophorin proteins. One third of band 3 particles (white particles), denoting band 3 dimers, are connected to the cytoskeleton. The rest of the band 3 particles (green particles) can freely diffuse in the lipid bilayer to simulate the mobile band 3 proteins. The CG particles, which form the

lipid bilayer and transmembrane proteins, carry both translational and rotational degrees of freedom ( $\mathbf{x}_i$ ,  $\mathbf{n}_i$ ), where  $\mathbf{x}_i$  and  $\mathbf{n}_i$  are the position and the orientation (direction vector) of particle  $i$ , respectively. The rotational degrees of freedom obey the normality condition  $|\mathbf{n}_i| = 1$ . Thus, each CG particle effectively carries 5 degrees of freedom.  $\mathbf{x}_{ij} = \mathbf{x}_j - \mathbf{x}_i$  is defined as the distance vector between particles  $i$  and  $j$ . Correspondingly,  $r_{ij} \equiv |\mathbf{x}_{ij}|$  is the distance, and  $\hat{\mathbf{x}}_{ij} = \mathbf{x}_{ij}/r_{ij}$  is a unit vector. The CG particles, forming the lipid membrane and membrane proteins, interact with one another via a pair-wise additive potential

$$u_{\text{mem}}(\mathbf{n}_i, \mathbf{n}_j, \mathbf{x}_{ij}) = u_R(r_{ij}) + A(\alpha, a(\mathbf{n}_i, \mathbf{n}_j, \mathbf{x}_{ij}))u_A(r_{ij}), \quad (2)$$

$$\begin{cases} u_R(r_{ij}) = k\epsilon \left( (R_{\text{cut,mem}} - r_{ij}) / (R_{\text{cut,mem}} - r_{eq}) \right)^8 - k\epsilon & \text{for } r_{ij} < R_{\text{cut,mem}} \\ u_A(r_{ij}) = -2k\epsilon \left( (R_{\text{cut,mem}} - r_{ij}) / (R_{\text{cut,mem}} - r_{eq}) \right)^4 - k\epsilon & \text{for } r_{ij} < R_{\text{cut,mem}} \\ u_R(r_{ij}) = u_A(r_{ij}) = 0, & \text{for } r_{ij} \geq R_{\text{cut,mem}} \end{cases} \quad (3)$$

where  $u_R(r_{ij})$  and  $u_A(r_{ij})$  are the repulsive and attractive components of the pair potential, respectively.  $\alpha$  is a tunable linear amplification factor. Fig. 6(a) shows that the applied potential in the case of  $A(\alpha, a) = +1$  has a wider energy well than the LJ6-12 potential, which facilitates CG particles pasting each other and thus enhance the fluidity of membrane. The function  $A(\alpha, a(\mathbf{n}_i, \mathbf{n}_j, \mathbf{x}_{ij})) = 1 + \alpha(a(\mathbf{n}_i, \mathbf{n}_j, \mathbf{x}_{ij}) - 1)$  tunes the energy well of the potential through which regulating the fluid-like behavior of the membrane, as shown in Fig. 6(b). In the simulations,  $\alpha$  was chosen to be 1.55 and cutoff distance of the potential  $R_{\text{cut,mem}}$  is chosen to be  $2.6\sigma$ . The parameters  $\alpha$  and  $R_{\text{cut,mem}}$  are selected to maintain the fluid phase of the lipid bilayer. The directionality of the CG particle is necessary for the self-assembly of the membrane sheet in the absence of solvent particles and lipid chains. The detailed information about applied potentials and the selection of the potential parameters can be found from authors' previous work [103, 104].

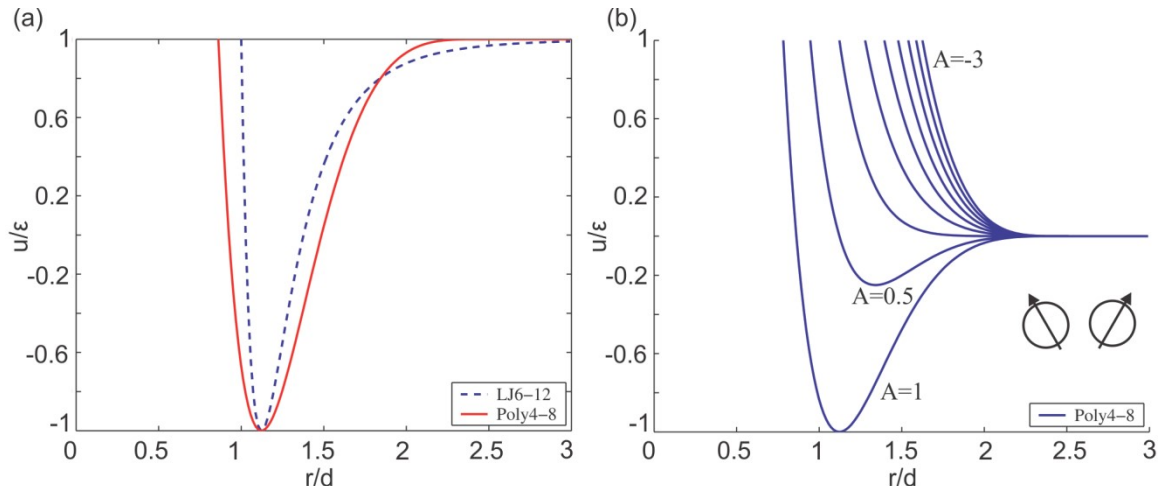


Figure 6. The pair-wise interaction potential expressed by Eq (3). (a) Comparison with LJ6-12 potential; (b) the interaction potential profile as a function of  $A(\alpha, a)$ . Adapted from <sup>[103, 106]</sup>.

This modified two-component membrane model is able to capture the molecular structures of the RBC membrane in both normal and defective states and thus has been applied to study membrane stiffness, the protein diffusion and membrane vesiculation (see Fig.7) in the healthy and pathological conditions <sup>[106-109]</sup>.

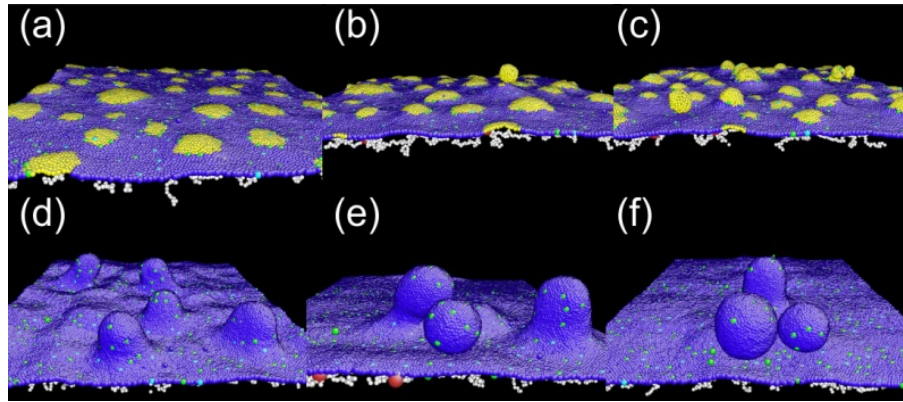


Figure 7. (a-c) Membrane budding and nanovesiculation induced by the spontaneous curvature of membrane domains (shown by the yellow particles). (a) When the spontaneous curvature is small, the membrane domains only bulge out from the membrane but no vesicle is formed. (b) As spontaneous curvature is increased, vesiculation occurs. (c) When spontaneous curvature is further increased, a larger number of vesicles are released from the membrane. (d-f) Vesiculation induced by lateral compression applied on the lipid bilayer (d) Only one protuberance is created at the beginning of the compression. (e) As the compression continues, the protrusion grows and a vesicle is formed. Then, a second protrusion is generated and the vesiculation process is repeated. (f) Finally, two vesicles are released from the membrane. Adapted from <sup>[106]</sup>

However, it was computationally expensive to scale up to large domains such as an entire RBC or whole blood involving large numbers of RBCs. To increase the length scale of the modified two-component membrane model, Tang et al. <sup>[110]</sup> recently developed OpenRBC, a multi-thread CGMD code, which is capable of simulating an entire RBC with explicit representations of lipid bilayer and cytoskeleton by multiple millions of CG particles using a single shared memory commodity workstation, as shown in Fig. 8.

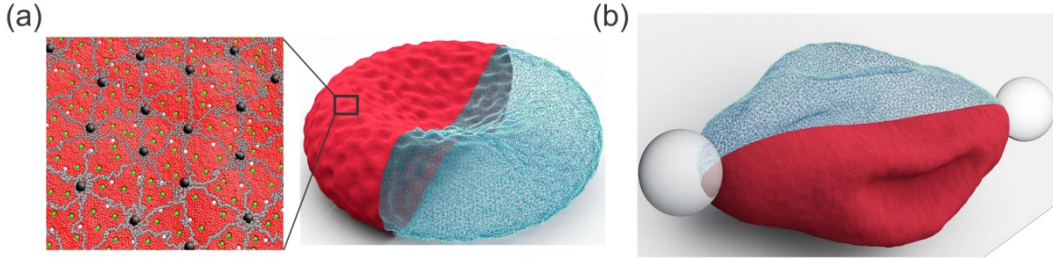


Figure 8. (a) OpenRBC can simulate the entire RBC based on the two-component RBC membrane model with explicit representations of lipid bilayer and cytoskeleton. Adapted from <sup>[110]</sup> (b) Simulation of optical tweezer experiment on a RBC by using OpenRBC. Adapted from <sup>[110]</sup>.

## 2.4 RBC whole cell models

Although OpenRBC allows us to simulate an entire RBC at protein resolution, it is still computationally prohibitively to simulate RBC suspensions and study the blood rheology. Thus, a more efficient RBC model with higher level of coarse-graining is required. Discher and co-workers <sup>[111]</sup> developed a CG particle model for the RBC membrane's spectrin cytoskeleton to the study the elasticity of RBC in micropipette aspiration. In this spectrin-level RBC model, a RBC is treated as a 2D canonical hexagonal network of CG particles (see Fig.9(a)) where the immediate neighbors are connected via a worm-like chain (WLC) potential, representing a spectrin filament. The bending rigidity induced by the lipid bilayer is represented by a bending potential applied between two triangles with a common side. In addition, surface area and cell column constrains are applied to represent the incompressibility of the lipid bilayer and cytosol. Li et al. <sup>[112]</sup> extended this model by incorporating the effects of random spectrin network, structural relaxation of the in-plane shear energy, and to the spontaneous curvature of the lipid bilayers. Pivkin et al. <sup>[113]</sup> introduced hydrodynamic effect into this elastic RBC model by combining it with DPD. More importantly, this RBC model is further coarse-grained from 23867 CG particles to 500 CG particles while the elastic properties are still preserved. This DPD-based whole cell model is computationally very efficient and it can be used not only in simulations of the single cell dynamics <sup>[114]</sup> and morphological changes of diseased RBC (see Fig.9(b)) <sup>[115]</sup>, but also the rheology of the blood flow <sup>[116, 117]</sup> and blood flowing through micro-devices (see Fig.9(c))<sup>[118]</sup>. However, it is not capable of modeling the interactions between the cytoskeleton and the lipid bilayer, which is frequently essential, as demonstrated in the study of the lipid bilayer detachment and RBC vesiculation. To overcome this issue, a RBC model consisting of two layers of 2D triangulated networks, where one layer represents the cytoskeleton and the other layer represents the lipid bilayer, was introduced to study of the interactions between the cytoskeleton and the lipid bilayer in healthy and diseased RBCs<sup>[119-121]</sup>. Both one-component and two-component whole-cell models take into account the elastic energy ( $V_s$ ), bending energy ( $V_b$ ), and constraints of fixed surface area ( $V_a$ ) and enclosed volume ( $V_v$ ) of an RBC, but bilayer-cytoskeleton interaction energy ( $V_{int}$ ) is additionally considered in two-component models.  $V_s$  mimics the elastic spectrin network, given by

$$V_s = \sum_{j \in 1 \dots N_s} \left[ \frac{k_B T l_m (3x_j^2 - 2x_j^3)}{4p(1-x_j)} + \frac{k_p}{(n-1)l_j^{n-1}} \right] \quad (4)$$

where  $l_j$  is the length of the spring  $j$ ,  $l_m$  is the maximum spring extension,  $x_j = l_j/l_m$ ,  $p$  is the persistence length,  $k_B T$  is the energy unit,  $k_p$  is the spring constant, and  $n$  is a specified exponent.  $V_b$  from the lipid bilayer of the RBC membrane is modeled by

$$V_b = \sum_{j \in 1 \dots N_s} k_b [1 - \cos(\theta_j - \theta_0)] \quad (5)$$

where  $k_b$  is the bending constant,  $\theta_j$  is the instantaneous angle between two adjacent triangles having the common edge  $j$ , and  $\theta_0$  is the spontaneous angle.  $V_a$  and  $V_v$  are imposed to mimic the area-preserving lipid bilayer and the incompressible interior fluid. The corresponding energys are given by

$$V_a = \sum_{j \in 1 \dots N_t} \frac{k_d (A_j - A_0)^2}{2A_0} + \frac{k_a (A_{\text{cell}} - A_{\text{cell},0}^{\text{tot}})^2}{2A_{\text{cell},0}^{\text{tot}}} \quad (6)$$

$$V_v = \frac{k_v (V_{\text{cell}} - V_{\text{cell},0}^{\text{tot}})^2}{2V_{\text{cell},0}^{\text{tot}}} \quad (7)$$

where  $N_t$  is the number of triangles in the membrane network,  $A_0$  is the triangle area, and  $k_d$ ,  $k_a$  and  $k_v$  are the local area, global area and volume constraint coefficients, respectively. The terms  $A_{\text{cell},0}^{\text{tot}}$  and  $V_{\text{cell},0}^{\text{tot}}$  represent the specified total area and volume, respectively. The bilayer-cytoskeleton interaction potential,  $V_{\text{int}}$ , is expressed as a summation of harmonic potentials given by

$$V_{\text{int}} = \sum_{j, j' \in 1 \dots N_{\text{bs}}} \frac{k_{\text{bs}} (d_{jj'} - d_{jj',0})^2}{2} \quad (8)$$

where  $k_{\text{bs}}$  and  $N_{\text{bs}}$  are the spring constant and the number of bond connections between the lipid bilayer and the cytoskeleton, respectively.  $d_{jj'}$  is the distance between the vertex  $j$  of the cytoskeleton and the corresponding projection point  $j'$  on the lipid bilayer, with the corresponding unit vector  $n_{jj'}$  and  $d_{jj',0}$  is the initial distance between the vertex  $j$  and the point  $j'$ , which is set to zero in the current simulations.

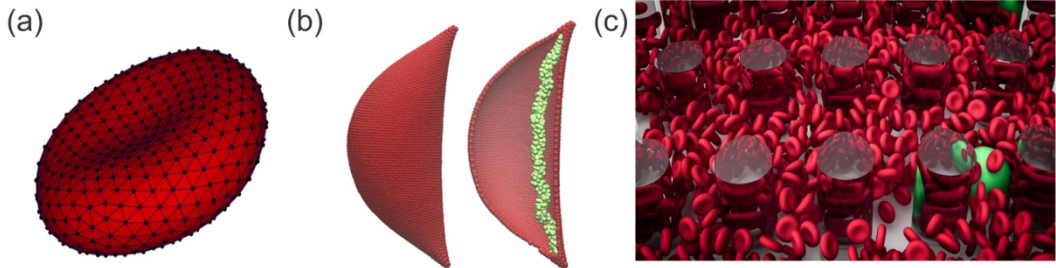


Figure 9. (a) A DPD whole cell model where RBC the membrane is modeled as a 2D canonical hexagonal network of DPD particles and the immediate neighboring DPD particles are connected via a WLC potential that represents a spectrin filament. (b) Application DPD whole cell model on simulation the cell morphology change due to the presence of sickle hemoglobin fibers in sickle cell disease. Adapted from <sup>[115]</sup>. (c) DPD whole cell model was applied to simulate RBCs passing pillar matrix on a microdevice. Adapted from <sup>[118]</sup>.

## 5. Summary

While atomistic simulations provide valuable and detailed information about the local structural properties of lipid membranes, they are limited to studying small patches of membrane of typically less than 100 nm because of computational costs. Many phenomena of biological interest are still outside of the range of these simulations in which individual atoms or lipid molecules are resolved. Continuum-based methods can treat much larger membrane or entire RBCs. However, they can not address problems concerning the detailed structural changes in the RBC membrane and specific protein defects in diseased RBCs. In addition, typical continuum mesh representations are not capable of appropriately modeling dramatic topology changes such as membrane budding, fusion, and self-assembly of lipid to vesicles. CG particle models are connected in certain aspects to both MD and continuum methods. On one hand, it is a discrete CG particle-based method like MD, but with each CG particle representing a blob or lump of molecules, instead of an atom or a molecule, thus simplifying the atomistic dynamics by eliminating fast degrees of freedom while preserving the mesoscopic structures and properties of membrane or RBCs, via which it provides an efficient simulation means to capture correct dynamics of membrane or RBCs at larger spatial and temporal scales. On the other hand, the CG particles may be considered as an extension of the mesh-free representation for continuum, but for 2D fluid membrane instead of 3D bulk fluid. Particularly, CG particle model can be used to simulate dynamical processes involve significant topological change, such as lipid particles self-assembly, vesicle fusion and nanoparticle transport through the erythrocyte membrane. It is worth noting that as the particles introduced in CGMD simulations do not correspond to real entities, the employed length scale and time scale do not have an immediate correlation with a physical system. Only through comparison with a natural procedure such a correspondence can be established. An emerging particle-based method, smoothed dissipative particle dynamics (SDPD) <sup>[122-124]</sup>, has also been applied to modeling rheology

of red and white blood cell behavior to elaborate the interaction of the surrounding fluid and membrane [125, 126]. SDPD method has advantages over conventional DPD, including well-defined physical scale of particles, direct inputs of transport properties and arbitrary equation of state. As an alternative of DPD, SDPD can be applied to study the transport phenomenon involved in the blood flows, such as drug delivering and cell loading in saline solution. However, it is more computationally expensive to perform SDPD simulations comparing to DPD simulations. Computational simulations have been playing an increasingly important role in enhancing our understanding of the dynamics and rheology of RBC suspensions in particular in blood diseases. The CG membrane and RBC models developed in the last decade have indeed been successfully employed to elucidate various membrane characteristics and functions. A complete picture of applications of CG particle models for membrane and RBC in physiological and pathological conditions and relevant references can be found in recent reviews [127-129].

## References

- [1] Alberts B, Johnson, A., Lewis, J., Ralf, M., Roberts, K., Walter, P. *Molecular Biology of the Cell*. New York: Garland. (2002)
- [2] Boal D. *Mechanics of the cell*. Cambridge, United Kingdom: Cambridge University Press. (2002)
- [3] Sten-Knudsen O. *Biological membranes: theory of transport, potentials and electric impulses*: Cambridge University Press. (2002)
- [4] Stillwell W. *An introduction to biological membranes: from bilayers to rafts*: Newnes. (2013)
- [5] Agre P. *Red Blood Cell Membranes: Structure: Function: Clinical Implications*: CRC Press. (1989)
- [6] Mohandas N, Evans E. Mechanical properties of the red cell membrane in relation to molecular structure and genetic defects. *Annual review of biophysics and biomolecular structure*, **23**(1), 787-818 (1994)
- [7] Feller SE. Molecular dynamics simulations of lipid bilayers. *Current Opinion in Colloid & Interface Science*, **5**(3-4), 217-23 (2000)
- [8] Saiz L, Bandyopadhyay S, Klein ML. Towards an understanding of complex biological membranes from atomistic molecular dynamics simulations. *Bioscience Reports*, **22**(2), 151-73 (2002)
- [9] Tieleman DP, Marrink SJ, Berendsen HJC. A computer perspective of membranes: molecular dynamics studies of lipid bilayer systems. *Biochimica Et Biophysica Acta-Reviews on Biomembranes*, **1331**(3), 235-70 (1997)
- [10] Tu KC, Klein ML, Tobias DJ. Constant-pressure molecular dynamics investigation of cholesterol effects in a dipalmitoylphosphatidylcholine bilayer. *Biophysical Journal*, **75**(5), 2147-56 (1998)
- [11] Hofsass C, Lindahl E, Edholm O. Molecular dynamics simulations of phospholipid bilayers with cholesterol. *Biophysical Journal*, **84**(4), 2192-206 (2003)

[12] Tieleman DP, Leontiadou H, Mark AE, Marrink SJ. Simulation of pore formation in lipid bilayers by mechanical stress and electric fields. *Journal of the American Chemical Society*, **125**(21), 6382-3 (2003)

[13] Canham PB. The minimum energy of bending as a possible explanation of the biconcave shape of the human red blood cell. *J Theoret Biol*, **26**, 61 - 81 (1970)

[14] Evans E. Bending resistance and chemically induced moments in membrane bilayers. *Biophysical Journal*, **14**, 923-31 (1974)

[15] Helfrich W. Elastic Properties of Lipid Bilayers - Theory and Possible Experiments. *Zeitschrift Fur Naturforschung C-a Journal of Biosciences*, **C 28**(11-1), 693-703 (1973)

[16] Seifert U. Configurations of fluid membranes and vesicles. *Advances in Physics*, **46**(1), 13-137 (1997)

[17] Smondyrev AM, Berkowitz ML. Molecular dynamics simulation of fluorination effects on a phospholipid bilayer. *Journal of Chemical Physics*, **111**(21), 9864-70 (1999)

[18] Zhao H, Isfahani AH, Olson LN, Freund JB. A spectral boundary integral method for flowing blood cells. *Journal of Computational Physics*, **229**(10), 3726-44 (2010)

[19] Veerapaneni SK, Rahimian A, Biros G, Zorin D. A fast algorithm for simulating vesicle flows in three dimensions. *Journal of Computational Physics*, **230**(14), 5610-34 (2011)

[20] Ramanujan S, Pozrikidis C. Deformation of liquid capsules enclosed by elastic membranes in simple shear flow: large deformations and the effect of fluid viscosities. *Journal of Fluid Mechanics*, **361**, 117-43 (1998)

[21] Lac E, Barthes-Biesel D, Pelekasis N, Tsamopoulos J. Spherical capsules in three-dimensional unbounded Stokes flows: effect of the membrane constitutive law and onset of buckling. *Journal of Fluid Mechanics*, **516**, 303-34 (2004)

[22] Peskin CS. The immersed boundary method. *Acta numerica*, **11**, 479-517 (2002)

[23] Doddi SK, Bagchi P. Three-dimensional computational modeling of multiple deformable cells flowing in microvessels. *Physical Review E*, **79**(4), 046318 (2009)

[24] Yazdani AZ, Bagchi P. Phase diagram and breathing dynamics of a single red blood cell and a biconcave capsule in dilute shear flow. *Physical Review E*, **84**(2), 026314 (2011)

[25] Fai TG, Griffith BE, Mori Y, Peskin CS. Immersed boundary method for variable viscosity and variable density problems using fast constant-coefficient linear solvers I: Numerical method and results. *SIAM Journal on Scientific Computing*, **35**(5), B1132-B161 (2013)

[26] Yazdani AZ, Kalluri RM, Bagchi P. Tank-treading and tumbling frequencies of capsules and red blood cells. *Physical Review E*, **83**(4), 046305 (2011)

[27] Salehyar S, Zhu Q. Deformation and internal stress in a red blood cell as it is driven through a slit by an incoming flow. *Soft matter*, **12**(13), 3156-64 (2016)

[28] Pozrikidis C. *Boundary integral and singularity methods for linearized viscous flow*: Cambridge University Press. (1992)

[29] Peng Z, Asaro RJ, Zhu Q. Multiscale modelling of erythrocytes in Stokes flow. *Journal of Fluid Mechanics*, **686**, 299-337 (2011)

[30] Venturoli M, Sperotto MM, Kranenburg M, Smit B. Mesoscopic models of biological membranes. *Physics Reports-Review Section of Physics Letters*, **437**(1-2), 1-54 (2006)

- [31] Drouffe JM, Maggs AC, Leibler S. Computer-Simulations of Self-Assembled Membranes. *Science*, **254**(5036), 1353-6 (1991)
- [32] Goetz R, Gompper G, Lipowsky R. Mobility and elasticity of self-assembled membranes. *Physical Review Letters*, **82**(1), 221-4 (1999)
- [33] Kumar PBS, Gompper G, Lipowsky R. Budding dynamics of multicomponent membranes. *Physical Review Letters*, **86**(17), 3911-4 (2001)
- [34] Noguchi H, Takasu M. Adhesion of nanoparticles to vesicles: A Brownian dynamics simulation. *Biophysical Journal*, **83**(1), 299-308 (2002)
- [35] Yamamoto S, Maruyama Y, Hyodo S. Dissipative particle dynamics study of spontaneous vesicle formation of amphiphilic molecules. *Journal of Chemical Physics*, **116**(13), 5842-9 (2002)
- [36] Farago O. "Water-free" computer model for fluid bilayer membranes. *Journal of Chemical Physics*, **119**(1), 596-605 (2003)
- [37] Marrink SJ, Mark AE. Molecular dynamics simulation of the formation, structure, and dynamics of small phospholipid vesicles. *Journal of the American Chemical Society*, **125**(49), 15233-42 (2003)
- [38] Marrink SJ, Mark AE. The mechanism of vesicle fusion as revealed by molecular dynamics simulations. *Journal of the American Chemical Society*, **125**(37), 11144-5 (2003)
- [39] Brannigan G, Philips PF, Brown FLH. Flexible lipid bilayers in implicit solvent. *Physical Review E*, **72**(1), (2005)
- [40] Cooke IR, Kremer K, Deserno M. Tunable generic model for fluid bilayer membranes. *Physical Review E*, **72**(1), (2005)
- [41] Laradji M, Kumar PBS. Domain growth, budding, and fission in phase-separating self-assembled fluid bilayers. *Journal of Chemical Physics*, **123**(22), 224902 (2005)
- [42] Laradji M, Kumar PBS. Dynamics of domain growth in multi-component self-assembled fluid vesicles in explicit solvent. *Biophysical Journal*, **88**(1), 239 (2005)
- [43] Markvoort AJ, Pieterse K, Steijaert MN, Spijker P, Hilbers PAJ. The bilayer-vesicle transition is entropy driven. *Journal of Physical Chemistry B*, **109**(47), 22649-54 (2005)
- [44] Wang ZJ, Frenkel D. Modeling flexible amphiphilic bilayers: A solvent-free off-lattice Monte Carlo study. *Journal of Chemical Physics*, **122**(23), (2005)
- [45] Brannigan G, Lin LCL, Brown FLH. Implicit solvent simulation models for biomembranes. *European Biophysics Journal with Biophysics Letters*, **35**(2), 104-24 (2006)
- [46] Markvoort AJ, van Santen RA, Hilbers PAJ. Vesicle shapes from molecular dynamics simulations. *Journal of Physical Chemistry B*, **110**(45), 22780-5 (2006)
- [47] Noguchi H, Gompper G. Meshless membrane model based on the moving least-squares method. *Physical Review E*, **73**(2), (2006)
- [48] Marrink SJ, Risselada HJ, Yefimov S, Tieleman DP, de Vries AH. The MARTINI force field: Coarse grained model for biomolecular simulations. *Journal of Physical Chemistry B*, **111**(27), 7812-24 (2007)
- [49] Muller M, Katsov K, Schick M. Biological and synthetic membranes: What can be learned from a coarse-grained description? *Physics Reports*, **434**(5-6), 113-76 (2006)
- [50] Kohyama T. Simulations of flexible membranes using a coarse-grained particle-based model with spontaneous curvature variables. *Physica a-Statistical Mechanics and Its Applications*, **388**(17), 3334-44 (2009)

[51] Muller M, Katsov K, Schick M. New mechanism of membrane fusion. *The Journal of Chemical Physics*, **116**(6), 2342-5 (2002)

[52] Ayton G, Voth GA. Bridging microscopic and mesoscopic simulations of lipid bilayers. *Biophysical Journal*, **83**(6), 3357-70 (2002)

[53] Yip S, Short MP. Multiscale materials modelling at the mesoscale. *Nature materials*, **12**(9), 774-7 (2013)

[54] Chang H-Y, Sheng Y-J, Tsao H-K. Structural and mechanical characteristics of polymersomes. *Soft Matter*, **10**(34), 6373-81 (2014)

[55] Li X, Pivkin IV, Liang H, Karniadakis GE. Shape transformations of membrane vesicles from amphiphilic triblock copolymers: a dissipative particle dynamics simulation study. *Macromolecules*, **42**(8), 3195-200 (2009)

[56] Li X, Guo J, Liu Y, Liang H. Microphase separation of diblock copolymer poly(styrene-b-isoprene): A dissipative particle dynamics simulation study. *The Journal of chemical physics*, **130**(7), 074908 (2009)

[57] Li X, Liu Y, Wang L, Deng M, Liang H. Fusion and fission pathways of vesicles from amphiphilic triblock copolymers: a dissipative particle dynamics simulation study. *Physical Chemistry Chemical Physics*, **11**(20), 4051-9 (2009)

[58] Chang H-Y, Chen Y-F, Sheng Y-J, Tsao H-K. Blending-induced helical morphologies of confined linear triblock copolymers. *Journal of the Taiwan Institute of Chemical Engineers*, **56**, 196-200 (2015)

[59] Lin Y-L, Chang H-Y, Sheng Y-J, Tsao H-K. Self-assembled polymersomes formed by symmetric, asymmetric and side-chain-tethered coil-rod-coil triblock copolymers. *Soft Matter*, **10**(11), 1840-52 (2014)

[60] Lin Y-L, Chang H-Y, Sheng Y-J, Tsao H-K. The fusion mechanism of small polymersomes formed by rod-coil diblock copolymers. *Soft matter*, **10**(10), 1500-11 (2014)

[61] Li H, Lykotrafitis G. A coarse-grain molecular dynamics model for sickle hemoglobin fibers. *Journal of the mechanical behavior of biomedical materials*, **4**(2), 162-73 (2011)

[62] Li H, Ha V, Lykotrafitis G. Modeling sickle hemoglobin fibers as one chain of coarse-grained particles. *Journal of biomechanics*, **45**(11), 1947-51 (2012)

[63] Zhang Y, Abiraman K, Li H, Pierce DM, Tzingounis AV, Lykotrafitis G. Modeling of the axon membrane skeleton structure and implications for its mechanical properties. *PLoS computational biology*, **13**(2), e1005407 (2017)

[64] Kim T, Hwang W, Lee H, Kamm RD. Computational analysis of viscoelastic properties of crosslinked actin networks. *PLoS Comput Biol*, **5**(7), e1000439 (2009)

[65] Kim T, Hwang W, Kamm R. Computational analysis of a cross-linked actin-like network. *Experimental Mechanics*, **49**(1), 91-104 (2009)

[66] Lu L, Li X, Vekilov PG, Karniadakis GE. Probing the twisted structure of sickle hemoglobin fibers via particle simulations. *Biophysical journal*, **110**(9), 2085-93 (2016)

[67] Lu L, Li H, Bian X, Li X, Karniadakis GE. Mesoscopic Adaptive Resolution Scheme (MARS) toward understanding of interactions between sickle cell fibers. *Biophysical Journal*, **112**(13), 2451-37 (2017)

[68] Brannigan G, Tamboli AC, Brown FLH. The role of molecular shape in bilayer elasticity and phase behavior. *Journal of Chemical Physics*, **121**(7), 3259-71 (2004)

[69] Yuan H, Huang C, Li J, Lykotrafitis G, Zhang S. One-particle-thick, solvent-free, coarse-grained model for biological and biomimetic fluid membranes. *Physical Review E*, **82**(1), 011905 (2010)

[70] Espanol P, Warren P. Statistical-Mechanics of Dissipative Particle Dynamics. *Europhys Lett*, **30**(4), 191-6 (1995)

[71] Hoogerbrugge PJ, Koelman J. Simulating Microscopic Hydrodynamic Phenomena with Dissipative Particle Dynamics. *Europhys Lett*, **19**(3), 155-60 (1992)

[72] Grafmuller A, Shillcock J, Lipowsky R. Dissipative particle dynamics of tension-induced membrane fusion. *Molecular Simulation*, **35**(7), 554-60 (2009)

[73] Brannigan G, Brown FLH. Solvent-free simulations of fluid membrane bilayers. *The Journal of Chemical Physics*, **120**(2), 1059-71 (2004)

[74] Marrink SJ, De Vries AH, Tieleman DP. Lipids on the move: simulations of membrane pores, domains, stalks and curves. *Biochimica et Biophysica Acta (BBA)-Biomembranes*, **1788**(1), 149-68 (2009)

[75] Lin C-M, Li C-S, Sheng Y-J, Wu DT, Tsao H-K. Size-dependent properties of small unilamellar vesicles formed by model lipids. *Langmuir*, **28**(1), 689-700 (2011)

[76] Lindahl E, Edholm O. Mesoscopic undulations and thickness fluctuations in lipid bilayers from molecular dynamics simulations. *Biophysical journal*, **79**(1), 426-33 (2000)

[77] Kranenburg M, Laforgue C, Smit B. Mesoscopic simulations of phase transitions in lipid bilayers. *Physical Chemistry Chemical Physics*, **6**(19), 4531-4 (2004)

[78] Kranenburg M, Smit B. Phase behavior of model lipid bilayers. *The Journal of Physical Chemistry B*, **109**(14), 6553-63 (2005)

[79] Tristram-Nagle S, Nagle JF. Lipid bilayers: thermodynamics, structure, fluctuations, and interactions. *Chemistry and physics of lipids*, **127**(1), 3-14 (2004)

[80] Lenz O, Schmid F. Structure of symmetric and asymmetric “ripple” phases in lipid bilayers. *Physical review letters*, **98**(5), 058104 (2007)

[81] Rodgers JM, Sørensen J, de Meyer FJ-M, Schiøtt B, Smit B. Understanding the phase behavior of coarse-grained model lipid bilayers through computational calorimetry. *The Journal of Physical Chemistry B*, **116**(5), 1551-69 (2012)

[82] Wu H-L, Sheng Y-J, Tsao H-K. Phase behaviors and membrane properties of model liposomes: Temperature effect. *The Journal of chemical physics*, **141**(12), 09B619\_1 (2014)

[83] Venturoli M, Smit B, Sperotto MM. Simulation studies of protein-induced bilayer deformations, and lipid-induced protein tilting, on a mesoscopic model for lipid bilayers with embedded proteins. *Biophysical journal*, **88**(3), 1778-98 (2005)

[84] Olbrich K, Rawicz W, Needham D, Evans E. Water permeability and mechanical strength of polyunsaturated lipid bilayers. *Biophysical Journal*, **79**(1), 321-7 (2000)

[85] Marrink SJ, De Vries AH, Mark AE. Coarse grained model for semiquantitative lipid simulations. *The Journal of Physical Chemistry B*, **108**(2), 750-60 (2004)

[86] Evans E, Rawicz W. Entropy-driven tension and bending elasticity in condensed-fluid membranes. *Physical Review Letters*, **64**(17), 2094 (1990)

[87] Nagle JF, Wilkinson DA. Dilatometric studies of the subtransition in dipalmitoylphosphatidylcholine. *Biochemistry*, **21**(16), 3817-21 (1982)

[88] Tristram-Nagle S, Wiener M, Yang C, Nagle J. Kinetics of the subtransition in dipalmitoylphosphatidylcholine. *Biochemistry*, **26**(14), 4288-94 (1987)

[89] Chernomordik LV, Kozlov MM. Protein-lipid interplay in fusion and fission of biological membranes. *Annual review of biochemistry*, **72**(1), 175-207 (2003)

[90] Liu J, Jiang X, Ashley C, Brinker CJ. Electrostatically mediated liposome fusion and lipid exchange with a nanoparticle-supported bilayer for control of surface charge, drug containment, and delivery. *Journal of the American Chemical Society*, **131**(22), 7567-9 (2009)

[91] Attwood SJ, Choi Y, Leonenko Z. Preparation of DOPC and DPPC supported planar lipid bilayers for atomic force microscopy and atomic force spectroscopy. *International journal of molecular sciences*, **14**(2), 3514-39 (2013)

[92] Wu H-L, Chen P-Y, Chi C-L, Tsao H-K, Sheng Y-J. Vesicle deposition on hydrophilic solid surfaces. *Soft Matter*, **9**(6), 1908-19 (2013)

[93] Lei G, MacDonald RC. Lipid bilayer vesicle fusion: intermediates captured by high-speed microfluorescence spectroscopy. *Biophysical journal*, **85**(3), 1585-99 (2003)

[94] García RA, Pantazatos SP, Pantazatos DP, MacDonald RC. Cholesterol stabilizes hemifused phospholipid bilayer vesicles. *Biochimica et Biophysica Acta (BBA)-Biomembranes*, **1511**(2), 264-70 (2001)

[95] Stevens MJ, Hoh JH, Woolf TB. Insights into the molecular mechanism of membrane fusion from simulation: evidence for the association of splayed tails. *Physical review letters*, **91**(18), 188102 (2003)

[96] Knecht V, Marrink S-J. Molecular dynamics simulations of lipid vesicle fusion in atomic detail. *Biophysical journal*, **92**(12), 4254-61 (2007)

[97] Smeijers A, Markvoort A, Pieterse K, Hilbers P. A detailed look at vesicle fusion. *The Journal of Physical Chemistry B*, **110**(26), 13212-9 (2006)

[98] Gao L, Lipowsky R, Shillcock J. Tension-induced vesicle fusion: pathways and pore dynamics. *Soft Matter*, **4**(6), 1208-14 (2008)

[99] Wu S, Guo H. Simulation study of protein-mediated vesicle fusion. *The Journal of Physical Chemistry B*, **113**(3), 589-91 (2008)

[100] Kozlovsky Y, Chernomordik LV, Kozlov MM. Lipid intermediates in membrane fusion: formation, structure, and decay of hemifusion diaphragm. *Biophysical journal*, **83**(5), 2634-51 (2002)

[101] Lin C-M, Wu DT, Tsao H-K, Sheng Y-J. Membrane properties of swollen vesicles: growth, rupture, and fusion. *Soft Matter*, **8**(22), 6139-50 (2012)

[102] Kuzmin PI, Zimmerberg J, Chizmadzhev YA, Cohen FS. A quantitative model for membrane fusion based on low-energy intermediates. *Proceedings of the National Academy of Sciences*, **98**(13), 7235-40 (2001)

[103] Li H, Lykotrafitis G. Two-component coarse-grained molecular-dynamics model for the human erythrocyte membrane. *Biophysical journal*, **102**(1), 75-84 (2012)

[104] Li H, Lykotrafitis G. Erythrocyte membrane model with explicit description of the lipid bilayer and the spectrin network. *Biophysical journal*, **107**(3), 642-53 (2014)

[105] Li J, Lykotrafitis G, Dao M, Suresh S. Cytoskeletal dynamics of human erythrocyte. *Proceedings of the National Academy of Sciences of the United States of America*, **104**(12), 4937-42 (2007)

[106] Li H, Lykotrafitis G. Vesiculation of healthy and defective red blood cells. *Physical Review E*, **92**(1), 012715 (2015)

[107] Li H, Zhang Y, Ha V, Lykotrafitis G. Modeling of band-3 protein diffusion in the normal and defective red blood cell membrane. *Soft matter*, **12**(15), 3643-53 (2016)

[108] Zhang Y, Huang C, Kim S, Golkaram M, Dixon MW, Tilley L, et al. Multiple stiffening effects of nanoscale knobs on human red blood cells infected with *Plasmodium falciparum* parasite. *Proceedings of the National Academy of Sciences*, **112**(19), 6068-73 (2015)

[109] Dearnley M, Chu T, Zhang Y, Looker O, Huang C, Klonis N, et al. Reversible host cell remodeling underpins deformability changes in malaria parasite sexual blood stages. *Proceedings of the National Academy of Sciences*, **113**(17), 4800-5 (2016)

[110] Tang Y-H, Lu L, Li H, Evangelinos C, Grinberg L, Sachdeva V, et al. OpenRBC: A Fast Simulator of Red Blood Cells at&#xa0;Protein Resolution. *Biophysical Journal*, **112**(10), 2030-7

[111] Discher DE, Boal DH, Boey SK. Simulations of the erythrocyte cytoskeleton at large deformation. II. Micropipette aspiration. *Biophysical Journal*, **75**(3), 1584-97 (1998)

[112] Li J, Dao M, Lim CT, Suresh S. Spectrin-level modeling of the cytoskeleton and optical tweezers stretching of the erythrocyte. *Biophysical Journal*, **88**(5), 3707-19 (2005)

[113] Pivkin IV, Karniadakis GE. Accurate coarse-grained modeling of red blood cells. *Physical review letters*, **101**(11), 118105 (2008)

[114] Pivkin IV, Peng Z, Karniadakis GE, Buffet PA, Dao M, Suresh S. Biomechanics of red blood cells in human spleen and consequences for physiology and disease. *Proceedings of the National Academy of Sciences*, **113**(28), 7804-9 (2016)

[115] Li X, Caswell B, Karniadakis George E. Effect of Chain Chirality on the Self-Assembly of Sickle Hemoglobin. *Biophysical Journal*, **103**(6), 1130-40 (2012)

[116] Fedosov DA, Pan W, Caswell B, Gompper G, Karniadakis GE. Predicting human blood viscosity in silico. *Proceedings of the National Academy of Sciences*, **108**(29), 11772-7 (2011)

[117] Fedosov DA, Noguchi H, Gompper G. Multiscale modeling of blood flow: from single cells to blood rheology. *Biomechanics and modeling in mechanobiology*, **13**(2), 239-58 (2014)

[118] Rossinelli D, Tang Y-H, Lykov K, Alexeev D, Bernaschi M, Hadjidoukas P, et al., The in-silico lab-on-a-chip: petascale and high-throughput simulations of microfluidics at cell resolution. *Proceedings of the International Conference for High Performance Computing, Networking, Storage and Analysis*; 2015.

[119] Peng Z, Li X, Pivkin IV, Dao M, Karniadakis GE, Suresh S. Lipid bilayer and cytoskeletal interactions in a red blood cell. *Proceedings of the National Academy of Sciences*, **110**(33), 13356-61 (2013)

[120] Li X, Peng Z, Lei H, Dao M, Karniadakis GE. Probing red blood cell mechanics, rheology and dynamics with a two-component multi-scale model. *Phil Trans R Soc A*, **372**(2021), 20130389 (2014)

[121] Chang H-Y, Li X, Li H, Karniadakis GE. MD/DPD multiscale framework for predicting morphology and stresses of red blood cells in health and disease. *PLoS Comput Biol*, **12**(10), e1005173 (2016)

[122] Espanol P, Revenga M. Smoothed dissipative particle dynamics. *Physical Review E*, **67**(2), 026705 (2003)

[123] Yang J. *A Smoothed Dissipative Particle Dynamics Methodology For Wall-Bounded Domains*. Ph.D Dissertation: Worcester Polytechnic Institute (2013).

- [124] Gatsonis NA, Potami R, Yang J. A smooth dissipative particle dynamics method for domains with arbitrary-geometry solid boundaries. *Journal of Computational Physics*, **256**, 441-64 (2014)
- [125] Fedosov DA, Peltomäki M, Gompper G. Deformation and dynamics of red blood cells in flow through cylindrical microchannels. *Soft matter*, **10**(24), 4258-67 (2014)
- [126] Fedosov DA, Gompper G. White blood cell margination in microcirculation. *Soft Matter*, **10**(17), 2961-70 (2014)
- [127] Li X, Li H, Chang H-Y, Lykotrafitis G, Karniadakis GE. Computational biomechanics of human red blood cells in hematological disorders. *Journal of Biomechanical Engineering*, **139**(2), 021008 (2017)
- [128] Li X, Dao M, Lykotrafitis G, Karniadakis GE. Biomechanics and biorheology of red blood cells in sickle cell anemia. *Journal of Biomechanics*, **50**, 34-41 (2017)
- [129] Li X, Vlahovska PM, Karniadakis GE. Continuum-and particle-based modeling of shapes and dynamics of red blood cells in health and disease. *Soft Matter*, **9**(1), 28-37 (2013)